Understanding Li interaction in TiO2/graphene composites for high-performance Li-ion battery anodes: A first principles study

El Hachimi, Abdel Ghafour

Elsevier B.V.
2023-07-01

El Hachimi, A G, Jiménez-Juárez, J A, Celaya, C A, Sundholm, D, Pyykkö, P & Muñiz, J
2023, 'Understanding Li interaction in TiO2/graphene composites for high-performance
Li-ion battery anodes: A first principles study', Physica B: Condensed Matter, vol. 660. https://doi.org/10.1016/j.physb

http://hdl.handle.net/10138/598548
10.1016/j.physb.2023.414878

Understanding Li interaction in TiO_2/graphene composites for high-performance Li-ion battery anodes: A first principles study

Abdel Ghafour El Hachimi[†a], Jesús A. Jiménez-Juárez[†a], Christian A. Celaya[a,c], Dage Sundholm[b], Pekka Pyykkö[b], and Jesús Muñiz[a]

[a] *Instituto de Energías Renovables, Universidad Nacional Autónoma de México, Priv. Xochicalco s/n, Col. Centro CP 62580, Temixco, Morelos, Mexico*
[b] *Department of Chemistry, Faculty of Science, University of Helsinki, P.O. Box 55, A. I. Virtasen aukio 1, FI-00014, Helsinki, Finland*
[c] *Centro de Nanociencias y Nanotecnología, Universidad Nacional Autónoma de México, Km 107 Carretera Tijuana-Ensenada, Ensenada, B.C., C.P. 22800, Mexico.*

Abstract

Composite materials consisting of TiO_2 and graphene (TiO_2/GR) have exciting properties that could make them suitable as anode material for Li-ion batteries. Systematic density functional theory (DFT) calculations were performed to investigate the TiO_2/GR energy-storage mechanism, adsorption sites and diffusion pathways of Li ions in TiO_2/GR. Its interface and the region outside graphene were studied for identifying stable surface sites. The adsorption energies are dominated by van der Waals interactions. Li diffusion along the graphene plane was the most favorable with a diffusion energy barrier of 0.24 eV, whereas the probability of diffusion at the

*Corresponding author
Email address: ag.elhachimi@ier.unam.mx (Abdel Ghafour El Hachimi[†])
†:These two authors contribute equally to the work.
Corresponding author. E-mail: jms@ier.unam.mx (Jesús Muñiz). Tel.: +52 (777) 362 0090

interface is low, due to the barrier of 3 eV. The composite exhibited a higher specific charge-storage capacity than other van der Waals heterostructures. The TiO_2/GR interface retains a large amount of charge implying that the TiO_2/GR composite shows suitable electrochemical properties for use as anode in lithium-ion batteries.
Keywords: LIB, DFT, TiO_2, Composite carbon structure, Graphene.

1. Introduction

The use of sustainable energy systems is essential to ensure an energy future based on renewable resources. The goal is that 85% of the consumed energy should in 2050 be renewable [1, 2]. It has been estimated that the electrochemical energy-storage capacity will increase from 195 GWh in 2019 to 2 TWh in 2030 [2]. Lithium-ion batteries (LIBs) will play an important role in the development of this technology. LIBs are aimed for short-term energy storage, whose maximum energy density is 300-750 kWh/m^3 [3] as compared to other energy-storage technologies such as capacitors (10-35 kWh/m^3), flywheels (0.3-400 kWh/m3), superconducting magnets (0.2-14 kWh/m^3) [4], compressed air (0.4-20 kWh/m^3), pumped hydroelectric storage (0.4-1.1 kWh/m^3), hydrogen fuel cells (500-3000 kWh/m^3), and thermal energy storage (800-500 kWh/m^3) [5]. Higher energy density, higher power, longer cyclic stability, and better thermal stability to a lower cost are necessary for future rechargeable batteries [6, 7]. Low-dimensional materials such as graphene-oxide, graphene-sulfide, and graphene-chloride nanostructures have been studied since they may be used in low-cost energy-storage devices [8–14].

Atomistic simulations are an important tool that allows the design of new battery materials with improved physico-chemical properties [15, 16]. Composite materials

of metal oxides and carbonaceous structures have a remarkably large storage capacity and a high electronic conductivity [17–22]. In particular, TiO_2 composites have been extensively studied due to their cyclic stability, low volume expansion and non-toxicity [16, 23], which holds for the anatase and the rutile crystal structures. The anatase structure has a good ionic diffusion and thermal stability [24, 25]. Experimental studies of anatase in a graphene composite material (TiO_2/GR) showed that they have a better storage capacity than pristine TiO_2. The use of nanocomposites based on the combination of graphene and metal oxide has been extensively studied for applications in energy storage [26–30]. In this context, among the most popular methods in the synthesis of the TiO_2/GR composites, the sol-gel and Hummers methods [28, 30] are widely known. The characterization techniques such as high-resolution transmission electron microscopy (HRTEM) and X-ray diffraction (XRD) have been used to evidence the phases of the nanocomposites. The performance of the composite material is still good after several charge/discharge cycles [20, 24, 31–34]. Fu *et al.* [33] reported a storage capacity of 568 mAh/g for a multilayer structure that reached a constant value of 175 mAh/g after 3000 cycles. The voltage range of the TiO_2/GR composite material ranges from 1.7 V to 3 V [24, 31], which is higher than that of graphite-based anodes [35]. First-principles calculations on TiO_2/GR yielded a smaller band gap [36–39] than for pristine TiO_2. Charge density calculations showed that van der Waals forces dominate the interaction between graphene and the TiO_2 nanoparticles (NP). Liu *et al.* [40] modeled insertion of Li ions into the composite material by calculating adsorption energies and charge densities. The most energetically stable site for insertion of Li ions was at the interface near the

oxygen atoms. Muñiz *et al.* [41] have studied the adsorption of TiO_2 clusters on a multi-walled carbon nanotube (MWCNT) using molecular dynamics simulations. They found a non-covalent interaction between the TiO_2 clusters and the multilayer carbon material as well as a strong intermolecular electrostatic-type C-O interaction.

Cai *et al.* [42] performed a combined experimental/theoretical study of a TiO_2-graphene composite, where graphene was grown on TiO_2 nanotubes forming a K-ion hybrid capacitor with an energy and power density of 81.2 Wh/kg and 3746.6 W/kg, respectively. The electronic conductivity was elucidated by using a TiO_2 molecular model interacting with the graphene monolayer. Calculations of the density of states showed that there is a change from semiconducting to metallic TiO_2 due to charge transfer from the graphene. A combined experimental/theoretical study of N-doped oxygen deficient TiO_{2-x}/reduced graphene oxide for use in Li/S batteries showed that the doping increased the adsorption of Li polysulfides, which was shown by calculating the adsorption energy of Li_2S_6 clusters grafted on pristine anatase TiO_2 and the adsorption energy for a defective TiO_{2-x} (101) surface. Seetharaman *et al.* [27] also performed an experimental/theoretical study of a supercapacitor electrode model consisting of TiO_2/carbon hybrids. They assessed the quantum capacitance of bulk TiO_2, surface TiO_2, and a model of TiO_2/reduced graphene. The quantum capacitance was found to be better for the composite material, which was attributed to the formation of electronic states that lead to a conducting TiO_2/carbon composite. DFT calculations by Zhu *et al.* [43] showed that the capacitance properties of the black titania/carbon composite material are enhanced as compared to those of

pristine TiO_2 due to the decrease in the Li^+ adsorption energy, which may be closely related to an easier Li diffusion than for pristine TiO_2. DFT calculations by Zou *et al.* [44] also showed that the H-TiO_{2-x}/C composite has a stable structure whose oxygen vacancies may result in low energy barriers and small adsorption energies for Na^+ ions.

Combined experimental and theoretical studies showed that the TiO_2/GR composite material could be used as anode material for LIBs, whereas a limited number of theoretical studies has been performed on TiO_2/GR interfaces and how they affect the energy-storage properties of the composite material. The diffusion pathways of the Li ions at the TiO_2/GR interface are still not elucidated. Here, we calculate electronic structure properties of a TiO_2/GR composite material at the DFT level. Li ions are inserted at different sites in the composite material and at the interface to estimate the diffusion pathways of the Li ions and the energy-storage capacity.

2. Computational details

The DFT calculations were performed at the generalized gradient approximation (GGA) level using the Perdew-Burke-Ernzerhof (PBE) functional [45, 46] as implemented in the Quantum ESPRESSO code [47]. The van der Waals interactions were introduced with Grimme's semi-empirical dispersion correction [48]. Particularly, the PBE-D2 [49] and PBE-D3 [50] functionals were used in benchmark calculations, which are described in section 3.1 below. The valence electrons C($2s^2 2p^2$), Ti($4s^2 3d^2$), O($2s^2 2p^4$), and Li ($2s^1$) were expanded in a plane-wave basis set with a cut-off energy of 400 eV. A supercell of $5 \times 5 \times 1$ was chosen, based on the unitary carbon

cells (40 carbon atoms). A spatial gap of 30 Å was introduced to avoid spurious interactions. A 2 × 2 × 1 Monkhorst-Pack k-point sampling grid was used in the structural relaxation. A 4 × 4 × 1 sampling grid was employed to obtain electronic structure properties. The electronic energy convergence of the self-consistent-field calculations was reached when the energy change was smaller than 1×10^{-4} Ry and the force reached a value of 0.01 eV/Å. This force threshold was also used in the structural optimizations. To elucidate the interaction of the TiO_2 model with the GR layer, several possible configurations were investigated. The lowest-energy configuration was considered to be the most stable structure. The adsorption energy was calculated using

$$E_{ads} = E_T(\mathrm{TiO_2/GR + Li}) - E_T(\mathrm{TiO_2/GR}) - E_T(\mathrm{Li}), \tag{1}$$

where $E_T(\mathrm{TiO_2/GR + Li})$ is the total energy of the Li ion adsorbed on the TiO_2/GR system. $E_T(\mathrm{TiO_2/GR})$ is the total energy of the TiO_2/GR system, and $E_T(\mathrm{Li})$ represents the total energy of an isolated Li atom in the same unit cell. The charge-density differences ($\Delta\rho$) were also studied using Bader's population analysis to elucidate the TiO_2 charge transfer on the GR substrate. The isosurface of the charge-density differences is given by

$$\Delta\rho = \rho_(\mathrm{adsorbent+substrate}) - \rho(\mathrm{adsorbent}) - \rho(\mathrm{substrate}) \tag{2}$$

where ρ(adsorbent+substrate) is the charge distribution of the Li ion adsorbed on the TiO_2/GR system. ρ(substrate) is the charge of the GR surface and $\rho(TiO_2)$ is

the charge density of the TiO_2 model. The average adsorption energy (E_{avg}) and open-circuit voltage (OCV) are extensively used to characterize battery performance. The battery health and the electronic charge storage are characteristic properties of battery performances [51]. The E_{avg} was computed as

$$E_{avg} = \frac{E_T(\text{substrate} + \text{Li}) - E_T(\text{substrate}) - nE_T(\text{Li})}{n}, \tag{3}$$

where n is the number of intercalated Li ions. The OCV profile is important since it is related to the energy-storage properties and to the total energy of the battery [52].

The OCV can be estimated by calculating the largest Li-ion retention in the system, *i.e.*, the OCV is given by

$$\text{OCV} = \frac{-E_{avg}}{e}, \tag{4}$$

where e is the elementary charge. The E_{avg} parameter has been successfully used in several studies [53] to assess the OCV values. The agreement in such works with the experimental data has been excellent. Consequently, the accuracy of the methodology is reliable without considering the zero point energy (ZPE) correction through Gibbs free energy calculations. This can directly be inferred since the OCV parameter does not depend on the temperature when assuming that the entropy and volume parameters can be neglected [54–56]. The energy-storage capacity was also estimated using

$$Q = 1000 \times F \times z\frac{n}{M_a}, \tag{5}$$

In Eq. 5; F, z, n and M_a are the Faraday constant (F is 26.801 Ah/mol) [51], z is the number of valence electrons ($z = 1$ for Li), n is the number of the intercalated Li ions, and M_a is the molar mass of the system without the ion. The study of the diffusion properties and the activation energies of Li adsorbed on the surface was performed with the nudged elastic band method (NEB) [57, 58]. The schematic diffusion pathways consist of seven images, which were evaluated at two initial positions. A convergence threshold of $1{\times}10^{-4}$ Ry was used for the total energy of the studied diffusion pathways. The convergence of the adsorption energy of the most stable TiO_2/GR composite configurations was checked by decreasing the energy threshold from 10^{-4} to 10^{-6} Ry. The obtained values with the two thresholds are 1.522 and 1.521 eV, respectively. Since the difference between the values is very small, all calculations were performed with the energy threshold of 10^{-4} Ry to speed up the computational time. For the TiO_2 system, it is relevant to consider the effect of the one-site Coulomb correction of the atomic $3d$ levels. Therefore, the GGA+U approach proposed by Dudarev *et al.* [59] was also used. An effective U value of 8.0 eV was used for the anatase structure as suggested by German *et al.* [60].

The electron density of the alloying mechanism as well as of the conversion and intercalation reactions were analyzed using the atoms in molecules (AIM) formalism [61]. The Bader AIM analysis was performed with the TURBOMOLE 6.6 program [62] at the DFT level using the PBE functional and the def2-SVP basis sets. The details of the employed AIM formalism are described in the Supporting Information

(SI). The temperature effect was also studied to assess the thermal stability. *Ab initio* molecular dynamics (AIMD) calculations were performed within the NVT ensemble at a temperature of 300 K. The full AIMD simulation time was 5 ps, with a time step of 1 fs. All AIMD simulations were performed with the VASP computational code [63–65].

3. Results and discussion

3.1. Structural description of theTiO_2/GR, TiO_2/GR/Li and TiO_2/Li/GR models

The model system used in the calculations consists of a TiO_2 semiconductor supported on a graphene monolayer as shown in Fig. 1. The anatase phase of the TiO_2 surface was chosen due to its good diffusivity and thermal stability. These properties have been studied for structures smaller than 200 nm [24]. It is important to highlight that in the molecular models, the anatase symmetry was implemented, since it has been shown [20] that Li-ion batteries based on TiO_2/carbon composite yielded an enhanced performance for anatase from that observed in rutile or brookite symmetries. This may be understood from the symmetrical arrangement in anatase, which exhibits wider tunnels where the ions are allowed to intercalate. This behavior is certainly limited in geometrical dispositions provided by rutile and brookite structures. Nevertheless, the ion diffusion pathways may also be explored for the combinations rutile/graphene, and brookite/graphene, but are out of the scope of the present work. The direction of the interaction between the TiO_2 model and the GR monolayer was chosen to be perpendicular to the (001) plane. A reduced surface model is necessary to optimize the computational costs and to speed up the conver-

gence of the DFT calculations. Periodic boundary conditions are used for the TiO_2 structure supported on the GR slab model. The TiO_2 model covers 37% of the GR surface, having a comparable size as the GR slab. There are experimental Atomic Layer Deposition (ALD) studies where a small portion of TiO_2 has been deposited on carbon as a solid thin film [66] suggesting that calculations on a moderate amount of TiO_2 on carbon may be enough to reproduce the most significant electronic structure properties. The TiO_2/carbon composite system has been experimentally studied with different carbon allotropes, such as MWCNT [20] and porous carbon [66]. TiO_2 was uniformly deposited on the GR layer. The lattice parameters of TiO_2 anatase and the carbon nanostructure do not match. This is also the case for porous carbon. In order to study such systems at the atomistic level, a cluster-type TiO_2 anatase was therefore used in the DFT calculations (see Fig. 1 (a)). This model is valid since the lattice parameters of both TiO_2 and GR are not modified in the calculations. A similar approach has previously been used in studies of other heterojunctions [67]. This approach may provide realistic electronic structure properties, which has been the case in studies of other systems [68]. The simplified model could represent experimentally studied electrode materials whose TiO_2 nanoparticles were deposited on MWCNTs using the controlled hydrolysis technique [20] or using the ALD method on porous carbon [66].

The electronic structure of the graphene monolayer has characteristic C-C bond lengths of 1.41 Å. To preserve the intrinsic properties of the GR monolayer, the TiO_2 model was supported on the GR monolayer with the unchanged structural parameters of the TiO_2 anatase, as shown in the inset in Fig. 1(a).

The TiO_2/GR interaction distance was estimated by performing single-point calculations of the energy for a number of structures with different distances between the graphene layer and TiO_2. A similar procedure was used for determining the equilibrium position of the Li ion adsorbed at the interface. The distance between the graphene monolayer and TiO_2 is 2.69 Å, which was obtained by fitting a Morse-type potential to the calculated energies. The edge sites were not saturated with hydrogen atoms because periodic conditions were imposed on the unit cell. The missing hydrogen atoms and their influence on the stability of the composite system was also tested. The interaction between the TiO_2 model system and graphene was thoroughly evaluated by varying the distance between them from 1.8 Å to 5.0 Å, which guarantees that a stable configuration can be found in this interval. The repulsion dominates at small separation distances (1.8 Å) and the attraction vanishes at a long distance (5.0 Å). The computed adsorption energy profile is depicted in Fig. 1(a). The dispersion data were fitted to a Morse potential by using a home-made Python code [69]. The Morse-type potential has been widely used to model the structural properties of extended graphene models and their interaction with different adsorbates [70–73]. Some results for the carbon models and their interactions agree rather well with those obtained at the DFT+D2 level of theory [74]. Thus, the employed methodology can be used for simulating the TiO_2/graphene interface. A comparison of the model stability was performed with PBE-D2, PBE-D3 and DFT+U(PBE-D3) functionals, which was our fastest computational level. The equilibrium distances obtained at these levels are 2.70, 2.62 and 2.93 Å, respectively. Since the difference between these values are small, we used the computationally robust and affordable

(PBE-D2) approach in the this work.

The equilibrium distance obtained at the PBE-D2 level is at 2.70 Å. A significant contribution of 1.52 eV to the binding energy can be directly attributed to van der Waals attraction as shown in Fig. 1(a). The energy minimum was obtained at 2.81 Å when the TiO_2 model was saturated with hydrogen atoms. Since the distances do not significantly differ, the calculations were performed only using the model without hydrogen saturation. Calculating the equilibrium distance at other levels of theory yielded similar results as shown in Fig. 1(a)). As a consequence, the Hubbard potential U does not play a significant role for the molecular structure. The structural calculations were therefore performed without the U term.

The Li ions were intercalated in the TiO_2/GR structure by considering several positions. The material with the Li ions adsorbed under the graphene monolayer is denoted (TiO_2/GR/Li), while the structure with the Li ions intercalated at the interface between TiO_2 and GR is denoted TiO_2/Li/GR. The sites of intercalation are called hollow (H), bridge (B), and top (T). See Fig. 1(b). The H sites are at the center of a six-membered ring of the graphene lattice; the B sites are at the C-C bonds; the T sites are at a carbon atom. The calculated adsorption energies for the sites are summarized in Table 1.

The adsorption energies of the Li ions in the TiO_2/GR/Li structure are -1.75, -1.41 and -1.43 eV for the H, B, and T sites, respectively. The equilibrium distances of the Li ion are 2.74, 2.74 and 2.75 Å for those sites. See Fig. 2(b),(d),(f). The adsorption energy for the H site is larger than for the Li ions on pristine graphene. An adsorption energy of -1.46 eV has been previously reported for Li ions adsorbed on

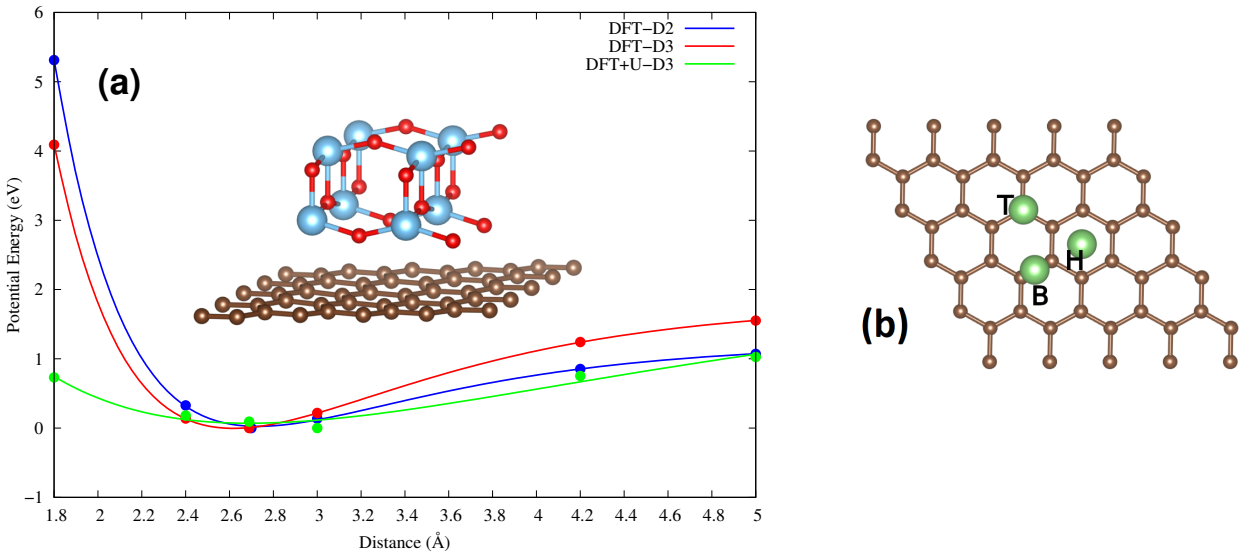

Figure 1: (a) Side view of the TiO_2/GR structure. Red, blue and brown balls represent the O, Ti and C atoms, respectively. The optimized distance between the graphene layer and the closest O atom is 2.69 Å. (b) The green balls represent the positions where the Li ions are intercalated.

graphene. [75]. The adsorption energies obtained in this work agree well with values calculated for other graphene-based heterostructures, such as phosphorene/graphene (P/GR/Li) [76] and antimonene/graphene (Sb/GR/Li),[77] whose adsorption energies at the H sites are -1.48 and -1.79 eV, respectively.

Calculations on TiO_2/Li/GR yielded adsorption energies of -3.33, -2.70 and -2.22 eV for the H, B and T sites, respectively. The obtained equilibrium distances are 2.67, 3.61 and 3.53 Å. See Fig. 2(a),(c),(e). The adsorption at the H site has the lowest energy. It is slightly larger than the one obtained in previous studies on P/Li/GR [76], and Sb/Li/GR [77], whose adsorption energies are -2.58 and -2.74 eV, respectively. The reported adsorption energy of Li ions on the TiO_2 anatase surface is -3.67 eV [78]. The calculated adsorption energies show that the Li ions are bound to the TiO_2/GR composite material at all adsorption sites.

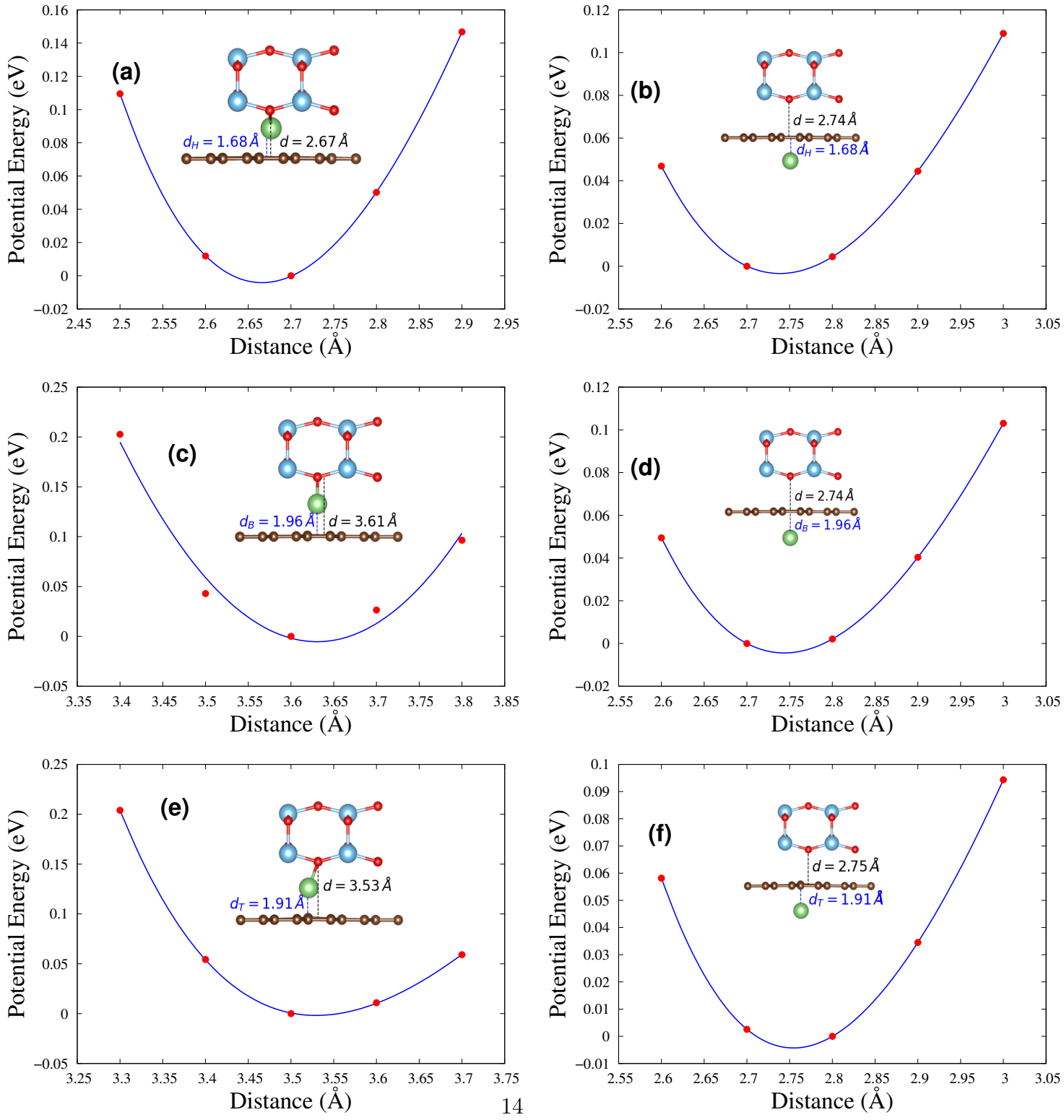

Figure 2: Side view of the optimized structures and the relative energy as a function of the distance between the graphene layer and the nearest O atom. The studied systems are TiO_2/Li/GR: (a) Hollow, (c) Bridge, (e) Top, and TiO_2/GR/Li: (b) Hollow, (d) Bridge, (f)Top.

Table 1: Partial Bader charges (in e) of the C, Ti, O and Li atoms. The equilibrium distances and adsorption energies of the Li ion adsorbed at the hollow (H), top (T) and bridge (B) sites of TiO_2/Li/GR and TiO_2/GR/Li are also given. The TiO_2/GR system is given as reference.

System	Sites	Q_{Li}	Q_C	Q_{Ti}	Q_O	d_{min}[Å]	E_{ads}[eV
TiO_2/GR	-	-	+0.068	+0.184	-0.253	2.69	-
TiO_2/Li/GR	H	+0.875	-0.431	-0.106	-0.337	2.67	-3.327
	B	+0.870	-0.441	-0.117	-0.312	3.61	-2.703
	T	+0.856	-0.424	-0.166	-0.265	3.53	-2.218
TiO_2/GR/Li	H	+0.861	-0.776	-0.031	-0.054	2.74	-1.752
	B	+0.814	-0.743	-0.027	-0.050	2.74	-1.412
	T	+0.819	-0.743	-0.029	-0.048	2.75	-1.423

3.1.1. Electronic structure properties of the studied systems

To understand the interactions in the studied system, we performed electronic structure calculations to determine the hybridization level of the C, Ti and O atoms in the TiO_2/GR composite material. The band-gap energies (E_g) were calculated for the three studied systems. Fig. 3(a) shows the total density of states (TDOS) of graphene, TiO_2 and TiO_2/GR. The DOS of graphene shows that it has a vanishing band-gap at the Dirac point of the Fermi level (E_F). This is related to the sp^2 hybridization of the C atoms in agreement with previous theoretical studies [22, 79]. Calculation of the DOS of TiO_2 showed that it has a band gap of approximately 1 eV. See Fig. 3(a). The obtained band gap of TiO_2 is smaller than the E_g of the TiO_2 bulk material of 3.20 eV [36, 38]. The smaller band gap can be attributed to the confinement effect of the reduced TiO_2 anatase clusters (see [80] and references therein).

The DOS of the TiO_2/GR system showed that this system has a smaller band gap than TiO_2. The band gap can be attributed to the hybridization of the valence

orbitals of the C atoms with the Ti and O orbitals. Similar results have been reported in previous studies [36, 37, 39, 81]. The smaller band gap of the composite material could also be related to the improved conductivity. Enhancement of the conductivity has been observed in experimental studies [20, 31–33, 82].

The partial density of states (PDOS) was also calculated for the TiO_2/GR composite material. Fig. 3(b) shows that the dominating states of the valence band are mainly formed from the O-2p orbitals. The hybrid orbitals consisting of contributions from the Ti-3d, O-2p and C-2p orbitals can also be identified in the energy range from -6.0 eV to 0.4 eV, which is in agreement with results obtained in a previous study [83]. The conduction band (CB) mainly consists of Ti-3d orbitals with a small contribution from the O-2p and C-2p orbitals. The C-2p states in the lower part of the CB lead to a narrowing of the band gap, which has also been considered to be related to its optoelectronic properties [38, 83, 84].

The PDOS was mapped to understand the interaction of the Li atoms intercalated in the TiO_2/GR/Li and TiO_2/Li/GR composite materials. The PDOS reveals contributions from the Li ions located at the H site. The PDOS of TiO_2/GR/Li in Fig. 3(c) has a large contribution from the Li-2s orbitals in the CB, suggesting that the Li ions introduce electronic states into this band. An overlap of the C-2p and Li-2s orbitals was also found in the CB suggesting that there is a strong electrostatic interaction between the C and Li atoms. The Fermi level is also close to the CB, indicating an excess of charge carriers in the composite material.

The PDOS of TiO_2/Li/GR is shown in Fig. 3(d). The Li ion is inserted at the interface of the composite material. There is a contribution from the Li-2s orbitals

in the CB and an overlap of the Li-2s and O-2p orbitals showing that there is an electrostatic interaction between the O and Li atoms.

The calculations reveal that the Li-2s orbitals of the Li ions in TiO_2/GR/Li have the largest contribution to the DOS of the composite material, which agrees with previous studies on graphene heterostructures.[18, 76, 77, 85] In antimonene/graphene composite materials, there is a larger contribution from the C(p) orbitals of GR to the CB of Li/GR/Sb as compared to GR/Li/Sb, [77] which was also obtained in computational studies on phosphorene/borophene composite materials (Li/P/B and P/Li/B) [85].

The isosurfaces representing the electron-density differences ($\Delta\rho$) for TiO_2/GR, TiO_2/Li/GR and TiO_2/GR/Li are shown in Fig. 4. The yellow regions represent electron accumulation, while depletion is shown in cyan. For TiO_2/GR in Fig. 4(a),(b), the electron transfer occurs from graphene at the interface of the composite between the C and O atoms to the TiO_2 surface leading to positively charged graphene. Electrons are accumulated near the O atoms resulting in a negative charge distribution on the isosurface that is shown in yellow. Electrons are also transferred from the Ti atoms as shown in cyan.

Figures 4(c) and (d) depict the TiO_2/Li/GR interaction. The charge is depleted at the surface between the C and the Li ions, and transferred to the TiO_2 surface. The interface between TiO_2 and GR has a significant charge transfer. A small charge transfer was identified at the TiO_2 surface.

In TiO_2/GR/Li (Fig. 4(f),(g)) the electron depletion is located to the Li ion. The region between the Li ion and the graphene surface shows electron accumulation,

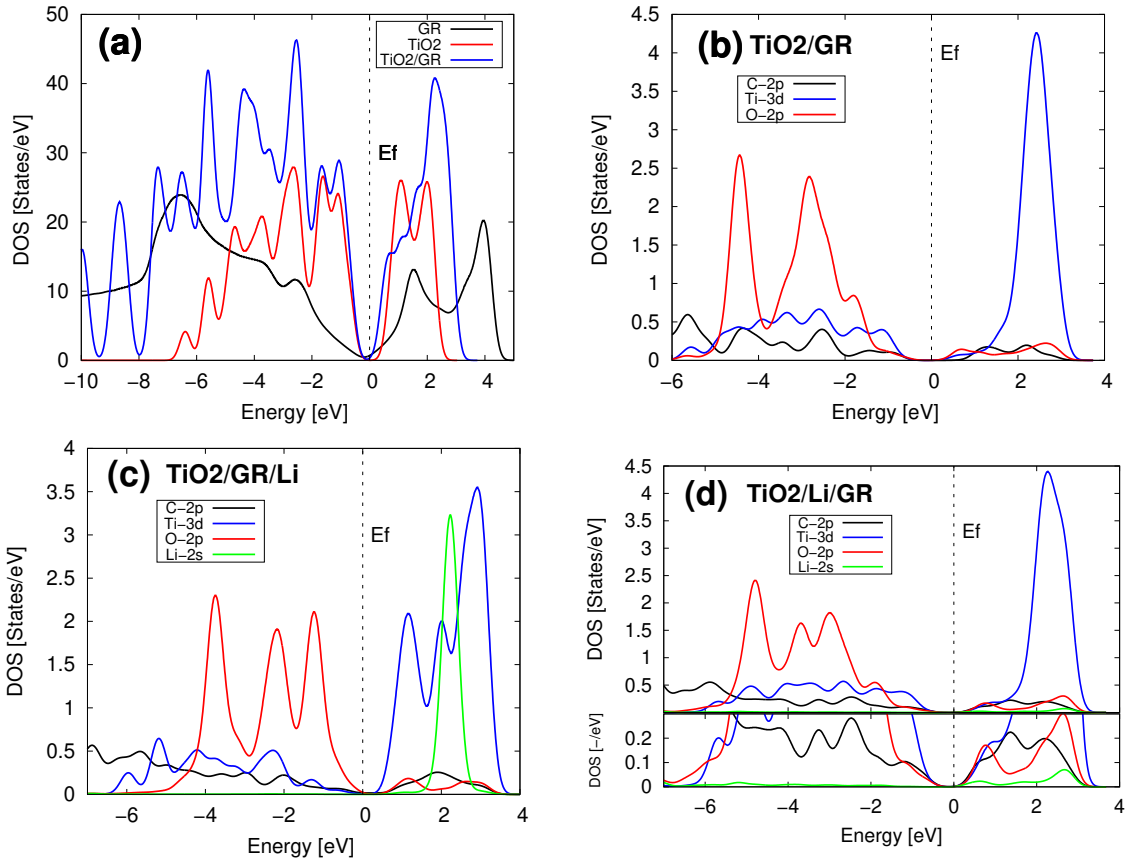

Figure 3: (a) Density of states (DOS) of GR, TiO_2 and the TiO_2/GR composite, (b) partial density of states (PDOS) of TiO_2/GR, (c) PDOS of TiO_2/GR/Li, (d) PDOS of TiO_2/Li/GR. The inset shows an amplification of the lowest DOS values.

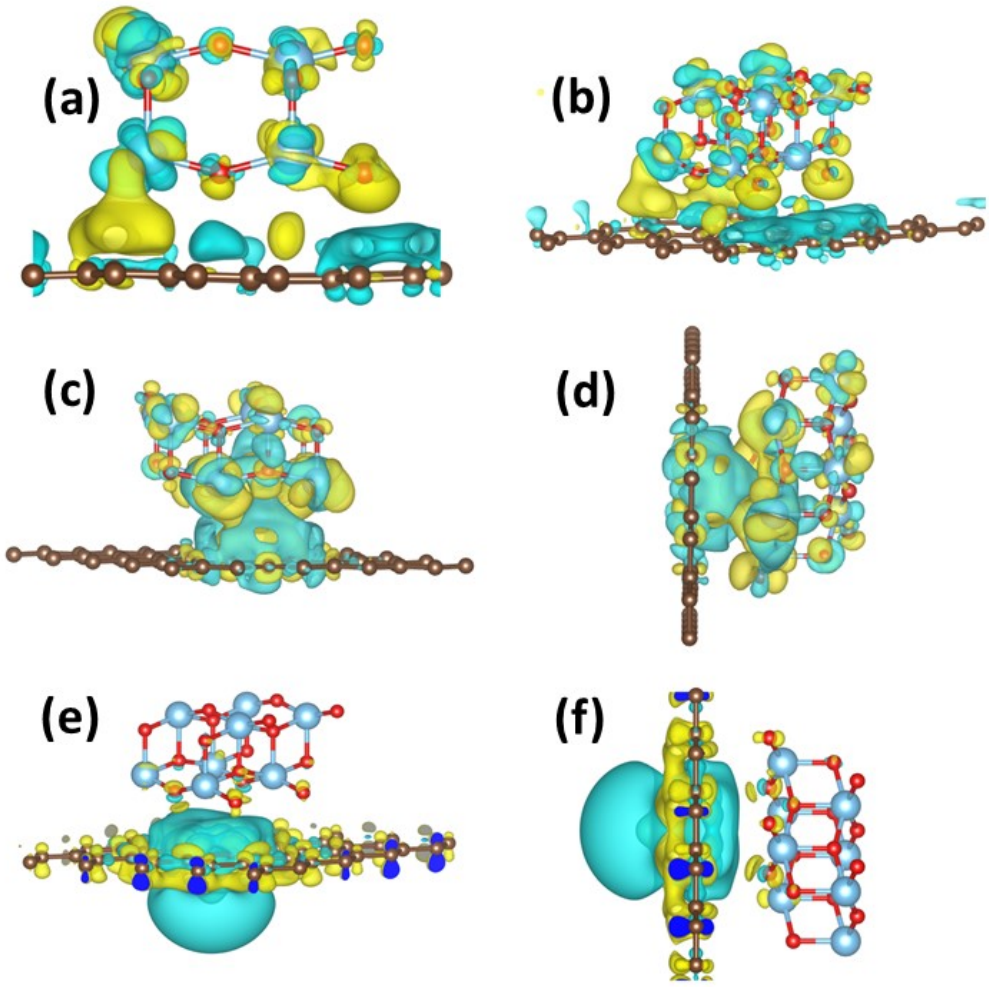

Figure 4: Electron density difference isosurfaces are shown. Cyan and yellow areas represent electron depletion and accumulation, respectively. The studied systems are TiO_2/GR: (a) side view, and (b) crystal orientation view. The isosurface value is 0.001 $e/Å^3$. TiO_2/Li(H)/GR: (c) crystal orientation view, and (d) side view. The isosurface value is 0.001 $e/Å^3$. TiO_2/GR/Li(H): (e) crystal orientation view, and (f) side view. The isosurface value is 0.0003 $e/Å^3$.

whereas there is electron depletion at the interface between the graphene surface and TiO_2. In TiO_2, electron accumulation appears around the O atoms. There is a small electron transfer to the lower layers of TiO_2, even though they are not in direct contact with the graphene surface.

The charge density averaged in the xy plane along the z-axis of TiO_2/GR/Li and TiO_2/Li/GR were also calculated and reported in Fig. S2 of the SI. In the density profile of TiO_2/Li/GR, there is a charge-density difference at the interface between the graphene surface and TiO_2. The charge profile of TiO_2/GR/Li shows electron depletion at the graphene surface.

Bader charge analysis was performed for TiO_2/GR, yielding charges of Q_C = +0.0684 $|e|$, Q_{Ti} = +0.1843 $|e|$ and Q_O = -0.2527 $|e|$, which agree with values estimated from the electronic charge-density isosurfaces discussed above. The largest charge states are found among the Ti and O atoms, which may be due to the ionic bonding in the TiO_2 surface.

The charge transfer between the graphene surface and the O atoms at the interface is small, since the interactions in this region are dominated by van der Waals forces. This is in agreement with results reported in previous computational studies of TiO_2 anatase structures on graphene, where it was shown that the graphene surface exhibits a charge depletion with atomic charges of +0.07 and +0.1 $|e|$ [37, 39]. The Bader charge analysis was also performed for TiO_2/Li/GR and TiO_2/GR/Li with Li ions in the H sites. The obtained charge difference of the elements are reported in Table 1. The calculations show that the largest electron transfer occurs at the H sites, which also agrees with results obtained with the electron localization

function (ELF) analysis reported in Fig. S3 of the SI. The ELF analysis shows that the electrons are localized to the sp^2 hybridized bonds of graphene. The Li ions affect the electron distribution between graphene and the TiO_2 structure by forming a large contribution of the ELF at the interface. The overall charge of the composite system is neutral. The initial neutral charge of Li, O, and Ti atoms changed in the geometry optimizations (see Table 1), whereas the total charge did not change. Since the Li atoms have a charge of +0.8492, we call it Li ion.

The Li ions at the H sites in TiO_2/Li/GR have a positive charge of +0.875 $|e|$ and a charge of -0.431 $|e|$ is transferred to the GR surface. TiO_2 has a negative charge of -0.443 $|e|$ of which -0.337 $|e|$ and -0.106 $|e|$ belong to the O and Ti atoms, respectively. The Li electrons are distributed at the interface between graphene and TiO_2, suggesting a charge polarization at the interface.

For TiO_2/GR/Li, the Li ion has a charge of +0.861 $|e|$. Its electrons are transferred to the GR surface resulting in a charge of -0.776 $|e|$. The Ti and O atoms have charges of -0.031 and -0.054 $|e|$, respectively. The charge transfer occurs at the GR surface, confirming ionic interactions as it was also observed in previous computational studies on GR heterostructures [76, 77].

AIM calculations were used for evaluating the bond critical points (BCP) in the TiO_2/GR composite system in the presence of Li. The AIM calculations described in the SI provide information about the reaction mechanisms of the anode material and might identify the alloying-conversion and intercalation mechanisms [52]. The AIM method was used for evaluating the BCP values for the optimized TiO_2/GR/Li and TiO_2/Li/GR structures. The BCP are shown in Fig. 5. TiO_2/GR/Li has a

BCP at the GR/Li interface. The obtained BCP values are summarized in Table 2. Two BCPs were obtained at the top and bottom regions of the Li interface of TiO_2/Li/GR, which indicates the presence of weak interactions. Based on the AIM analysis, TiO_2/GR/Li and TiO_2/Li/GR seem to have intercalation-reaction processes.

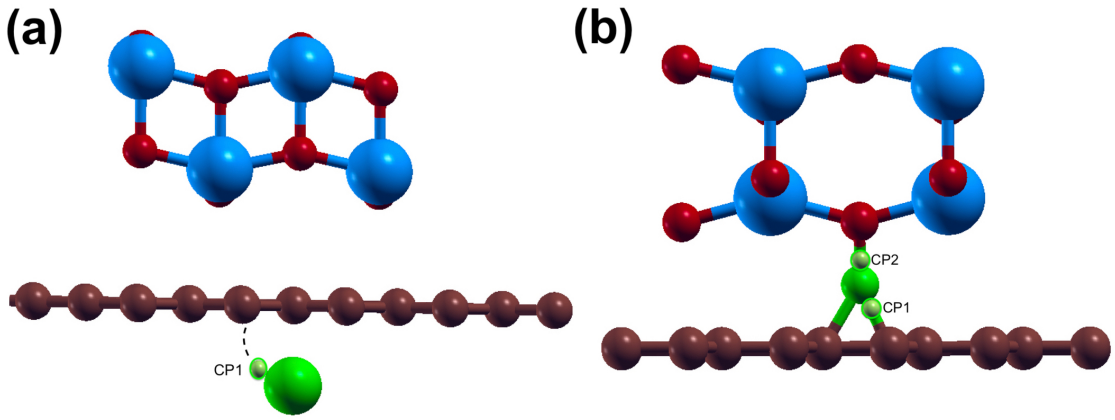

Figure 5: AIM critical points (light green balls) in the composite systems: (a) TiO_2/GR/Li and (b) TiO_2/Li/GR.

Table 2: AIM values of the bond critical points (BCP) for TiO_2/GR/Li and TiO_2/Li/GR

System	ρ (r_{bcp}) (a.u)	$\nabla^2\rho$ (r_{bcp}) (a.u.)
TiO_2/GR/Li – BCP1	0.048	0.033
TiO_2/Li/GR – BCP1	0.127	1.008
TiO_2/Li/GR – BCP2	0.066	0.631

3.2. Theoretical voltage and specific capacity

Full optimization of structures with a large number of intercalated Li ions on TiO_2/GR was performed to assess the maximum capacity of the system. Different concentrations of nLi were evaluated, where n= 8, 16, 24, 32, 40, 48, 56 and 64. The largest number of Li ions is limited by the available sites. The H sites were considered as initial positions before the optimization. For $n \geq 56$, also the T sites were considered. The OCV was calculated using Eq. 4. The theoretical specific capacity for each concentration was calculated using Eq. 5. The relationship between the voltage and the specific capacity is shown in Fig. 6. The voltage has a step-like behavior with increasing Li concentration. The system with n=8 has a specific capacity of Q=173 mAh/g and a voltage of 3.34 V. For n=64, the specific capacity is Q=1384 mAh/g and a voltage of 1.83 V. These systems have voltages of 3.34 and 1.83 V, respectively, which are higher than for other composite structures [52, 77]. These results should be considered with caution, since the enhanced specific capacity of 1384 mAh/g could be due to structural deformation of graphene after Li-ion saturation. This behavior is shown in Fig. 6 (c). In this respect, the enhanced specific capacity could be compromised with a certain degree of distortion on the GR layer, which may represent a limitation on the performance of the battery. Alternatively, the implementation of different chemical compositions, such as $Li_{1.3}V_{0.4}Nb_{0.3}O_2$ and $Li_{1.25}V_{0.55}Nb_{0.2}O_{1.9}F_{0.1}$ may dramatically mitigate the former issue, since they represent zero-strain systems for battery cathodes [86]. The absence of volume changes in the cathode is intimately related to improved performance of the material. Such theoretical results were also certified via the experimental characterization of the

cathode with *in situ* XRD measurements. Specific capacities of the same order of magnitude have been previously obtained in computational studies on other systems such as boron phosphide (1283 $mAhg^{-1}$) [87], silicene (954 $mAhg^{-1}$) [88] and Sn (994 $mAhg^{-1}$) [89]. A specific capacity of 1130 mAh/g has also been obtained experimentally by Fu *et al.* [33]. This value was obtained in the first charge/discharge cycle when using a TiO_2/carbon anode composite material [33]. The results suggest that increasing the number of Li ions is related to a bonding tendency of the TiO_2 structure by an intrinsic interaction, while the Li-C bond is sufficiently effective for Li intercalation in the studied systems. The charge of the O and Ti atoms allows an attraction of Li ions that weakens the repulsion of the negative charges. However, lithiation with a high Li content causes distortions in the TiO_2 surface.

Based on the slight distortion by the TiO_2 structure during the process of maximum charge (64 Li), the thermal stability could be considered another descriptor to assess anode materials. Thus, AIMD simulations were performed for the TiO_2/GR system both prior and at the end of the storage charge process. Fig. S4 shows the evolution of the TiO_2/GR, TiO_2/Li/GR, and TiO_2/GR/64Li systems throughout 5 ps of AIMD simulation at the fixed temperature of 300 K. Both TiO_2/GR and TiO_2/Li/GR systems exhibited a small energy fluctuation (2 eV) after the 3 ps of the AIMD simulation (Fig. S4 (a) and (b)). The structural changes in the TiO_2 cluster are evident. However, the Ti-O bond is not dissociated, since the initial chemical composition (TiO_2) is maintained throughout the AIMD simulation. In addition, the temperature effect provokes the TiO_2 detachment from the GR surface. Nevertheless, this magnitude of separation is smaller for the TiO_2/Li/GR system, in which

the presence of the Li ion shows a higher affinity to interact with the TiO_2 structure. The origin of such separation may be strongly related to the weak interaction between the anatase structure and the GR surface. The effect of temperature on the TiO_2/GR/64Li system maintains structural stability between the TiO_2 cluster and the GR monolayer. In this system, the energy fluctuation reaches a small value of 3 eV after 3 ps in the AIMD simulation (See Fig. S4(c)). It is noteworthy to note that in all systems evaluated with AIMD simulations, the GR monolayer exhibits slight distortions. In order to give insight into the thermal stability of all systems under study, video clips of the AIMD simulation were also included in the SI. At the largest charge configuration, the TiO_2/GR/64Li system shows acceptable thermal stability, which could be strongly related to those experimentally evaluated in this type of composite [26].

As a further remark, it is known [90] that the optimal range of temperatures in which a LIB ensures environmental sustainability is from -40°C to 60°C. Temperature values above 60°C; namely 75°C, correspond to the melting point of ethylene carbonate (EC) electrolyte. At a temperature of 115°C, the breakdown of the solid electrolyte interphase (SEI) is also observed. Both phenomena have a detrimental effect in the overall performance of the battery. The incorporation of the electrolyte into the simulations of the present work is definitely out of the scope. Nevertheless, it is of interest to explore the behavior of the systems under study subjected to temperatures at operational conditions that do not compromise the intrinsic structure of the given materials. That is, further AIMD calculations were performed up to 60°C to elucidate the evolution of the TiO_2/carbon material, as it is incorporated in a LIB.

Such calculations were performed for the same series of systems previously studied at room temperature; namely TiO_2/GR, TiO_2/Li/GR and TiO_2/GR/64Li. This set of simulations were performed by subjecting the system for 5 ps at an applied constant temperature of 60 °C (333 K). The systems were then allowed to evolve at this given temperature by 5 ps.The energy profiles describing this procedure are shown in Fig. S5 (a) - (c) of SI.

The systems TiO_2/GR and TiO_2/Li/GR also revealed an energy stabilization starting at 1 ps (see Fig. S5 (a) and (b) of SI), with small energy fluctuations amounting to 1 eV and 1.5 eV for systems TiO_2/GR and TiO_2/Li/GR, respectively. It indicates that the systems are virtually unaltered at these given temperatures. It is worth mentioning that the TiO_2 structure in the TiO_2/GR system was subjected to a slight modification coming from an interaction between a Ti atom and a C center onto GR. Nevertheless, such modification does not alter the overall energy of the system as it is shown in Fig. S5 (a) of SI. Moreover, the system subjected to a temperature of 60 °C with a massive number of Li-ions adsorbed in the composite TiO_2/GR/64Li, also revealed an analogous behavior than that reported for room temperature. This behavior also addresses the thermal stability of the composite material subjected to extreme operating conditions if it were implemented as a LIB anode. It is important to highlight that the top temperature of 60 °C, as observed for LIBs operating with EC as the electrolyte, is justified in the evaluation of the systems under study, since the composite material TiO_2/carbon has been experimentally implemented as an anode material in LIBs, operating with EC as the electrolyte [20]. The video clips of these simulations were also included in the SI.

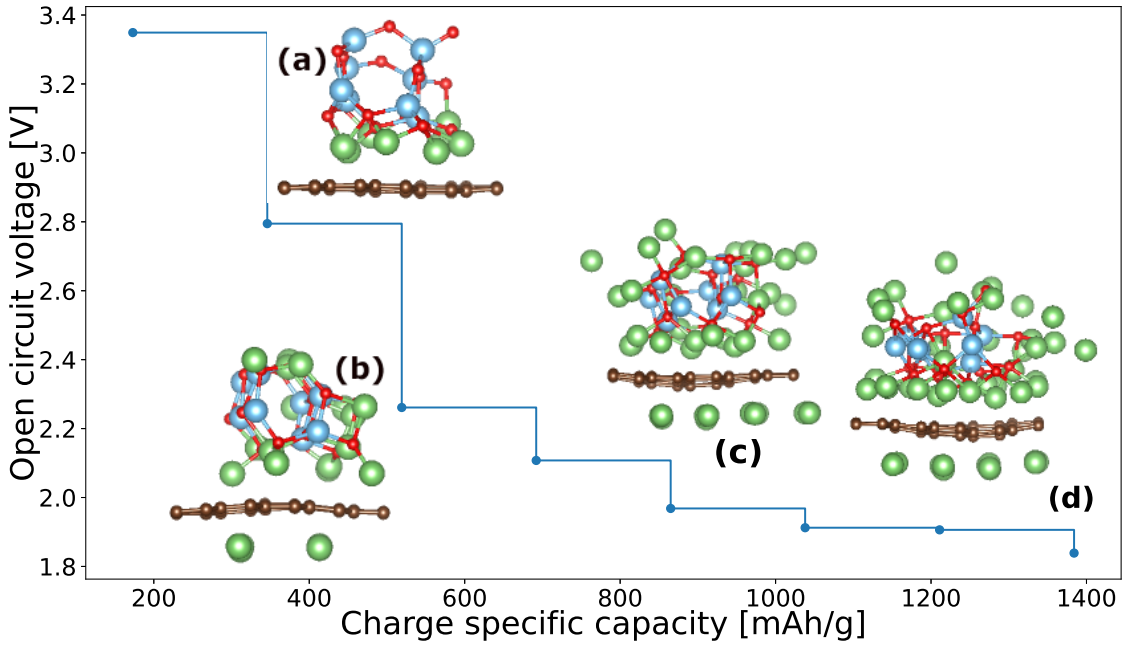

Figure 6: Open circuit voltage as a function of the specific capacity. The lithiated TiO_2/GR with different number of ions and its average adsorption energy (E_{avg}) are shown, (a) 8 Li^+ ions, E_{avg}=-3.35 eV, (b) 24 Li^+ ions, E_{avg}=-2.26 eV, (c) 48 Li^+ ions, E_{avg}=-1.91 eV, (d) 64 Li^+ ions, E_{avg}=-1.84 eV. Color code: brown, blue, red and lime balls correspond to C, Ti, O and Li atoms, respectively.

3.3. Diffusion pathways of Li ions and NEB calculations

Li diffusion is related to the battery charge/discharge performance [52]. Calculations of the Li diffusion were then performed using the NEB methodology. Energy barriers were calculated for different pathways to understand the diffusion character of the Li ions along these pathways. The H sites are the most stable when adsorbing Li ions onto TiO_2/GR. The Li diffusion from the H sites was modeled to explore possible energy barriers along the pathways. Three diffusion trajectories of the Li ion were chosen: (*i*) inside the TiO_2 structure, (*ii*) at the interface, and (*iii*) under the graphene monolayer of the TiO_2/GR system.

Fig. 7(a) and (b) illustrate case (*iii*). The pathway is chosen from one H site to another H location passing through two top sites (H→ T→B→T→H). The energy barrier for this pathway is 0.24 eV, which is comparable to the diffusion energy of Li on a graphene/phosphorene monolayer [22, 75, 91]. Similar results were obtained for other heterostructures such as Sb/GR/Li and borophene/GR/Li. Energy barriers of 0.34 and 0.25 eV were obtained for the diffusion below the graphene monolayer [76, 77]. Even when the pathway is symmetric with respect to the graphene surface, the energy curve of the transition states is not necessarily symmetric, which could be due to irregular van der Waals interactions between the Ti and O atoms with the graphene surface.

We also examined the interface between TiO_2 and GR. The Li ions follow the H→B→H path in Fig. 7(c),(d), where the B site is the least stable with an energy barrier of 3.0 eV. Regardless of the initial and final positions of the Li ion, it remained at the H site with different relative energy values. Particularly, the location

H corresponded to the site with the highest stability, which could be attributed to a stronger interaction of the Li ion with the O and Ti atoms in the initial position. The energy barriers at the interface are larger than in those cases where the Li ion remains below the TiO_2/GR composite. This may be attributed to the interactions of the Li ion with TiO_2 and GR.

Fig. 7 (e) and (f) describe the pathway inside TiO_2 from one octahedral O site to another. The Li ion migrates through the midpoint (M) which is the transition state with the largest energy. The pathway is then symmetric with an energy barrier of 0.79 eV. This value is similar to those reported in the 0.48-0.63 eV range. It agrees with previously reported values for the migration of Li ions in TiO_2 [92, 93].

We have used a simplified theoretical model for understanding the electronic structure properties of the composite material without omitting relevant information due to the atomistic treatment. The TiO_2/GR interface interaction is mediated by a weak attraction of the hydrogen bonding type according to the AIM calculations. Such an interaction is able to induce an electron transfer between the TiO_2 and the GR layer. The diffusion pathways calculated with the NEB methodology suggest a plausible mechanism for the Li-ion diffusion in the composite material. The most probable pathways of the Li-ion are below the TiO_2/GR interface and pass through the TiO_2 tunnels of the anatase structure, suggesting that intercalation represents the dominant mechanism of the ion transport. The diffusion below the GR layer may also contribute to the overall diffusion. Diffusion along the interface can definitely be ruled out due to the large activation energies. The weak interactions in the composite material prevent the transport of the Li ion at the interface.

It is worth mentioning that the energy barrier amounting to 0.79 eV corresponds to the diffusion pathway inside the TiO_2 anatase structure, which is comparable to other energy barriers observed in anode materials implemented for batteries [52, 94]. That is, the Sb_2S_3/S-doped carbon [52] and MoN_2 [94] showed energy barriers of 0.69 and 0.56 eV, respectively. Additionally, they showed adequate capacity and OCV values for energy storage applications. Moreover, the energy barriers are increased at the interface (see Fig. 7), which could be interpreted as a diffusion route with a small probability to be feasible in a charge/discharge cycle. Nevertheless, the most probable diffusion pathways are expected to be found at those regions where the Li-ion directly interacts with the carbon structure of the TiO_2/GR composite. In those sites the energy barriers are significantly decreased, amounting to 0.24 eV, which is even comparable with the barriers of 2D materials, such as Ti_2CSi_2 [95] and ReS_2 [53], with energy barriers amounting to 0.22 and 0.16 eV, respectively. This may be interpreted as the overall capacity of the composite material that allows the Li-ion diffusion to be enhanced at those regions that directly interact with carbon in the TiO_2/GR anode material.

With the aid of the present calculations, it was identified that the TiO_2 system and the graphene model share an interaction of the vdW-type that allows the stability on the composite material. As it was previously discussed in the present work, the diffusion pathways of the Li-ion which were found at the interface between the TiO_2 model and graphene appeared to be marginal. That is, the activation energies at those locations exhibited large values (see Fig. 7). As a consequence, the vdW-interaction could not be related to the Li-ion diffusion. Nevertheless, upon

evaluation of the diffusion pathways below the TiO_2/GR composite model, lower activation energies were assessed, which can be directly interpreted as an improvement in the energy storage process. Consequently, the combination of TiO_2 with carbon (exhibiting a mechanism of interaction) may certainly improve the energy storage processes, but it is not strictly related to the rising of the vdW-attraction. Nonetheless, the directionality of the ion-diffusion at the geometry of the TiO_2/carbon system may be a condition to improve the energy storage properties. Additionally, other mechanisms, such as quantum capacitance may also be responsible for an enhanced total capacitance, as it has already been observed upon carbon combination with other metal oxides [27].

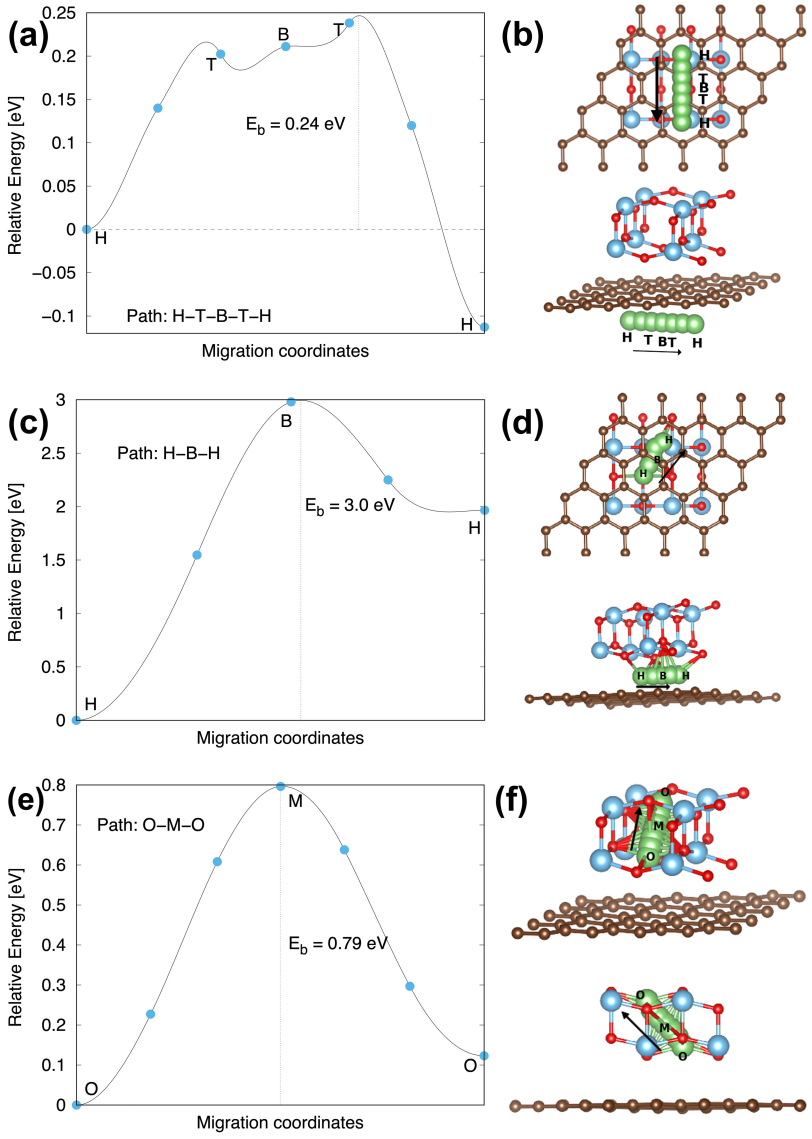

Figure 7: Diffusion pathways and energy barriers of the Li ions. (a) TiO_2/GR/Li, (c) TiO_2/Li/GR and (e) inside TiO_2. Graphical representation of the minimum energy pathways (b) of TiO_2/GR/Li: H→T→B→T→H , (d) of TiO_2/Li/GR: H→B→H and (f) inside TiO_2:O→M→O.

4. Conclusions

The role of the TiO_2 structure on a graphene monolayer and the Li ions storage capacity were computationally studied at the DFT-D2 level. Insertion of Li ions into the TiO_2/GR composite materials was investigated by considering several interaction positions at the TiO_2/GR interface and at the graphene on the outside of the composite. The most stable site (most exothermic) was found at the interface. The covalent bonding character is dominated by interactions between Li-C and Li-Ti/O atoms. The calculated adsorption energies yielded the strongest interactions of -3.33 and -1.75 eV, which correspond to the hollow positions of the interface and outside the composite material, respectively. The nature of this interaction was also corroborated by AIM analysis, showing different bond critical points. The composite material was found to support a large number of charge/discharge cycles due to its high specific capacity of 1384 mAh/g. Additionally, AIMD simulation evidenced the structural stability of the TiO_2/GR/64Li system at 300 K (during 5 ps). The system can operate in the voltage range from 1.85 to 3.35 eV. Such a high voltage is due to synergistic electronic effects of the graphene and TiO_2 providing an adequate performance during the lithiation/delithiation cycle, which could also lead to an effective intercalation reaction and a large storage capacity. NEB calculations for three pathways of the Li-ion diffusion in the composite structure showed that outside the graphene surface, the mobility of Li ions is improved as compared to the interface or inside the TiO_2 lattice. The results provide an atomistic-scale understanding of the Li-ion insertion to TiO_2/GR composite materials. The results also confirm that the TiO_2/GR composite represents a system for an efficient performance as an

electrochemical anode material implemented in LIB devices.

5. Acknowledgements

The authors would like to acknowledge the financial support given by DGAPA-UNAM (Dirección General de Asuntos del Personal Académico) under Project No. PAPIIT-(IG100720 and IN106122). J.M. would like to acknowledge the Supercomputing Department of Universidad Nacional Autónoma de México for the computing resources under Project No. LANCAD-UNAM-DGTIC-370, LANCAD-UNAM-DGTIC-310, LANCAD-UNAM-DGTIC-427 and the support given by Fondo Sectorial de Investigación para la Educación-CONACYT under Project No. A1-S-13294; Fronteras de la Ciencia-CONACYT under Project No. 21077. Project No. 270810 (Laboratorio Nacional de Conversión y Almacenamiento de Energía-CONACYT) and CIC-UNAM (Project No. COIC/STIA/8854/2019) are also acknowledged. C.A.C. wants to acknowledge DGAPA-UNAM for the postdoctoral fellowship. We acknowledge CSC - IT Center for Science, Finland, and the Finnish Grid and Cloud Infrastructure (persistent identifier urn:nbn:fi:research-infras-2016072533) for computational resources. The authors want to thank the technical support on high performance computing given by Kevin Alquicira Hernández.

6. CRediT authorship contribution statement

A.G. El Hachimi: Investigation, Methodology, Conceptualization, Software, Writing - Original Draft. **J.A. Jiménez-Juárez:** Investigation, Conceptualization, Methodology, Visualization. **C.A. Celaya:** Methodology, Visualization. **D. Sund-**

holm: Writing - Review & Editing, Formal analysis. **P. Pyykkö:** Writing - Review & Editing, Formal analysis. **J. Muñiz:** Supervision, Project Administration, Funding Acquisition, Writing - Review & Editing, Formal analysis.

7. Declaration of Competing Interest

The authors declare that they have no known competing financial interests or personal relationships that could influence the work reported in this paper.

References

[1] B. Hirschl, International renewable energy policy—between marginalization and initial approaches, Energy Policy 37 (11) (2009) 4407–4416.

[2] D. Gielen, F. Boshell, D. Saygin, M. D. Bazilian, N. Wagner, R. Gorini, The role of renewable energy in the global energy transformation, Energy Strategy Reviews 24 (2019) 38–50.

[3] F. Meishner, D. U. Sauer, Wayside energy recovery systems in dc urban railway grids, eTransportation 1 (2019) 100001.

[4] H. Chen, T. N. Cong, W. Yang, C. Tan, Y. Li, Y. Ding, Progress in electrical energy storage system: A critical review, Progress in Natural Science 19 (3) (2009) 291–312.

[5] S. Koohi-Fayegh, M. Rosen, A review of energy storage types, applications and recent developments, Journal of Energy Storage 27 (2020) 101047.

[6] B.-L. Xu, S.-H. Qi, M.-M. Jin, X.-Y. Cai, L.-F. Lai, Z.-T. Sun, X.-G. Han, Z.-F. Lin, H. Shao, P. Peng, Z.-H. Xiang, J. E. ten Elshof, R. Tan, C. Liu, Z.-X. Zhang, X.-C. Duan, J.-M. Ma, 2020 roadmap on two-dimensional materials for energy storage and conversion, Chinese Chemical Letters 30 (12) (2019) 2053–2064.

[7] B. Scrosati, History of lithium batteries, Journal of Solid State Electrochemistry 15 (7) (2011) 1623–1630.

[8] Q. He, B. Yu, Z.-H. Li, Y. Zhao, Density functional theory for battery materials, Energy & Environmental Materials 2 (4) (2019) 264–279.

[9] S. Shaheen Shah, S. M. Abu Nayem, N. Sultana, A. J. Saleh Ahammad, M. Abdul Aziz, Preparation of sulfur-doped carbon for supercapacitor applications: A review, ChemSusChem 15 (2022) e202101282.

[10] X. Wu, F.-Y. Kang, W.-H. Duan, J. Li, Density functional theory calculations: A powerful tool to simulate and design high-performance energy storage and conversion materials, Progress in Natural Science: Materials International 29 (3) (2019) 247–255, special Issue of Computational Materials.

[11] J.-X. Huang, G. Csányi, J.-B. Zhao, J. Cheng, V. L. Deringer, First-principles study of alkali-metal intercalation in disordered carbon anode materials, J. Mater. Chem. A 7 (2019) 19070–19080.

[12] J. Liu, S. Wang, Q. Sun, All-carbon-based porous topological semimetal for Li-ion battery anode material, Proceedings of the National Academy of Sciences 114 (4) (2017) 651–656.

[13] T. Jeon, S. Lee, S. C. Jung, Boron-, nitrogen-, aluminum-, and phosphorus-doped graphite electrodes for non-lithium ion batteries, Current Applied Physics 20 (8) (2020) 988–993.

[14] C.-F. Yang, C. Qiao, Y. Chen, X.-Q. Zhao, L.-L. Wu, Y. Li, Y. Jia, S.-Y. Wang, X.-L. Cui, Nitrogen doped γ-graphyne: A novel anode for high-capacity rechargeable alkali-ion batteries, Small 16 (10) (2020) 1907365.

[15] T. Osaka and Z. Ogumi, Nanostructure Science and Technology, in: Nanoscale Technology for Advanced Lithium Batteries, Vol. 1, Springer, New York, NY, 2014, pp. 1–273.

[16] M. Madian, A. Eychmüller, L. Giebeler, Current advances in TiO_2-based nanostructure electrodes for high performance lithium ion batteries, Batteries 4 (7) (2018).

[17] A. Yoshino, Development of the lithium-ion battery and recent technological trends, in: G. Pistoia (Ed.), Lithium-Ion Batteries, Elsevier, Amsterdam, 2014, pp. 1–20.

[18] J.-C. Ma, J. Fu, M.-Q. Niu, R. Quhe, MoO_2 and graphene heterostructure as promising flexible anodes for lithium-ion batteries, Carbon 147 (2019) 357–363.

[19] J.-H. Zhang, G. Liu, H.-C. Hu, L.-Y. Wu, Q. Wang, X.-J. Xin, S.-J. Li, P.-F. Lu, Graphene-like carbon-nitrogen materials as anode materials for Li-ion and Mg-ion batteries, Applied Surface Science 487 (2019) 1026–1032.

[20] P. Acevedo-Peña, M. Haro, M. E. Rincón, J. Bisquert, G. Garcia-Belmonte, Facile kinetics of Li-ion intake causes superior rate capability in multiwalled carbon nanotube@TiO_2 nanocomposite battery anodes, Journal of Power Sources 268 (2014) 397–403.

[21] C.-J. Chen, Y.-W. Wen, X.-L. Hu, X.-L. Ji, M.-Y. Yan, L.-Q. Mai, P. Hu, B. Shan, Y.-H. Huang, Na^+ intercalation pseudocapacitance in graphene-coupled titanium oxide enabling ultra-fast sodium storage and long-term cycling, Nature Communications 6 (2015) 1–8.

[22] D. H. Wu, Y. F. Li, Z. Zhou, First-principles studies on doped graphene as anode materials in lithium-ion batteries, Theoretical Chemistry Accounts 130 (2) (2011) 209–213.

[23] C.-H. Jiang, J.-S. Zhang, Nanoengineering titania for high rate lithium storage: A review, Journal of Materials Science & Technology 29 (2) (2013) 97 – 122.

[24] U. Farooq, F. Ahmed, S. A. Pervez, S. Rehman, M. A. Pope, M. Fichtner, E. P. Roberts, A stable TiO_2-graphene nanocomposite anode with high rate capability for lithium-ion batteries, RSC Advances 10 (50) (2020) 29975–29982.

[25] B. Zachau-Christiansen, K. West, T. Jacobsen, S. Atlung, Lithium insertion in different TiO_2 modifications, Solid State Ionics 28-30 (1988) 1176 – 1182.

[26] J. Qiu, C. Lai, Y. Wang, S. Li, S. Zhang, Resilient mesoporous TiO_2/graphene nanocomposite for high rate performance lithium-ion batteries, Chemical Engineering Journal 256 (2014) 247–254.

[27] A. Seetharaman, M. Kandasamy, S. Manivannan, K. Jothivenkatachalam, K. Subramani, A. Pandikumar, M. Sathish, V. Rao Soma, D. Sivasubramanian, B. Chakraborty, TiO_2/Carbon allotrope nanohybrids for supercapacitor application with theoretical insights from density functional theory, Applied Surface Science 563 (2021) 150259.

[28] Z. Li, Z. Liu, X. Yang, A. Chen, P. Chen, L. Yang, C. Yan, Y. Shi, Enhanced Photocatalysis of Black TiO_2/Graphene Composites Synthesized by a Facile Sol–Gel Method Combined with Hydrogenation Process, Materials 15 (9) (2022).

[29] Y. Zhao, H. Hao, T. Song, X. Wang, C. Li, W. Li, MnO_2-graphene based composites for supercapacitors: Synthesis, performance and prospects, Journal of Alloys and Compounds 914 (2022) 165343.

[30] S. Kumar, M. Kumawat, T. Mohanty, Tailoring surface electronic properties of GO-TiO_2 hybrid nanostructures through interface modifications, Applied Surface Science 609 (2023) 155398.

[31] D. Wang, D. Choi, J. Li, Z. Yang, Z. Nie, R. Kou, D. Hu, C. Wang, L. V. Saraf, J. Zhang, I. A. Aksay, J. Liu, Self-assembled TiO_2-graphene hybrid nanostructures for enhanced Li-ion insertion, ACS Nano 3 (4) (2009) 907–914.

[32] Y.-J. Cen, Y.-Q. Yao, Q. Xu, Z.-H. Xia, R. D. Sisson, J.-Y. Liang, Fabrication of TiO_2–graphene composite for the enhanced performance of lithium batteries, RSC Adv. 6 (2016) 66971–66977.

[33] W. Fu, Y. Li, M. sung Chen, Y. Hu, B. Liu, K. Zhang, C. Zhan, M. Zhang, Z. Shen, An orderly arrangement of layered carbon Nanosheet/TiO_2 nanosheet stack with superior artificially interfacial lithium pseudocapacity, Journal of Power Sources 468 (2020) 228363.

[34] J. Wang, Y.-K. Zhou, B. Xiong, Y.-Y. Zhao, X.-J. Huang, Z.-P. Shao, Fast lithium-ion insertion of TiO_2 nanotube and graphene composites, Electrochimica Acta 88 (2013) 847–857.

[35] Y.-D. Shen, J.-S. Chen, J.-X. Zhu, Q.-Q. Yan, X. Hu, Growth of two-dimensional ultrathin anatase TiO_2 nanoplatelets on graphene for high-performance lithium-ion battery, Journal of Nanoparticle Research 15 (10) (2013) 1913.

[36] Y. Masuda, G. Giorgi, K. Yamashita, DFT study of anatase-derived TiO_2 nanosheets/graphene hybrid materials, Physica Status Solidi (B) Basic Research 251 (8) (2014) 1471–1479.

[37] S. B. Mishra, S. C. Roy, B. Nanda, Electronic structure of graphene/TiO_2 interface: Design and functional perspectives, Applied Surface Science 542 (2021) 148709.

[38] P. Martins, C. Ferreira, A. Silva, B. Magalhães, M. Alves, L. Pereira, P. Marques, M. Melle-Franco, S. Lanceros-Méndez, TiO_2/graphene and TiO_2/graphene oxide nanocomposites for photocatalytic applications: A computer modeling and experimental study, Composites Part B: Engineering 145 (2018) 39–46.

[39] B. Bukowski, N. A. Deskins, The interactions between TiO_2 and graphene

with surface inhomogeneity determined using density functional theory, Physical Chemistry Chemical Physics 17 (44) (2015) 29734–29746.

[40] E.-Z. Liu, J.-M. Wang, C.-S. Shi, N.-Q. Zhao, C.-N. He, J.-J. Li, J.-Z. Jiang, Anomalous interfacial lithium storage in graphene/TiO_2 for lithium ion batteries, ACS Applied Materials & Interfaces 6 (20) (2014) 18147–18151.

[41] J. Muñiz, M. E. Rincón, P. Acevedo, The role of the oxide shell on the stability and energy storage properties of MWCNT@TiO_2 nanohybrid materials used in Li - ion batteries, Theoretical Chemistry Accounts 135 (7) (2016) 1–9.

[42] J. Cai, R. Cai, Z. Sun, X. Wang, N. Wei, F. Xu, Y. Shao, P. Gao, S. Dou, J. Sun, Confining TiO_2 Nanotubes in PECVD-Enabled Graphene Capsules Toward Ultrafast K-Ion Storage: In Situ TEM/XRD Study and DFT Analysis, Nano-Micro Letters 12 (1) (2020) 123.

[43] G.-Y. Zhu, L.-B. Ma, H.-N. Lin, P.-Y. Zhao, L. Wang, Y. Hu, R.-P. Chen, T. Chen, Y.-R. Wang, Z.-X. Tie, Z. Jin, High-performance Li-ion capacitor based on black-TiO^{2-x}/graphene aerogel anode and biomass-derived microporous carbon cathode, Nano Research 12 (7) (2019) 1713–1719.

[44] D. Zou, W. Wang, J. Liu, J. Weng, J. Duan, J. Zhou, P. Zhou, Insights into the storage mechanism of novel mesoporous hollow TiO_{2-x}/C nanofibers as a high-performance anode material for sodium-ion batteries, Carbon 194 (2022) 248–256.

[45] J. P. Perdew, K. Burke, M. Ernzerhof, Perdew, Burke, and Ernzerhof reply, Physical Review Letters 80 (4) (1998) 891.

[46] J. P. Perdew, K. Burke, M. Ernzerhof, Generalized gradient approximation made simple, Physical Review Letters 77 (18) (1996) 3865.

[47] P. Giannozzi, S. Baroni, N. Bonini, M. Calandra, R. Car, C. Cavazzoni, D. Ceresoli, G. L. Chiarotti, M. Cococcioni, I. Dabo, et al., Quantum espresso: a modular and open-source software project for quantum simulations of materials, Journal of physics: Condensed matter 21 (39) (2009) 395502.

[48] F. Ortmann, F. Bechstedt, W. Schmidt, Semiempirical van der Waals correction to the density functional description of solids and molecular structures, Physical Review B 73 (20) (2006) 205101.

[49] S. Grimme, Semiempirical GGA-type density functional constructed with a long-range dispersion correction, Journal of Computational Chemistry 27 (15) (2006) 1787–1799.

[50] S. Grimme, J. Antony, S. Ehrlich, H. Krieg, A consistent and accurate ab initio parametrization of density functional dispersion correction (DFT-D) for the 94 elements H-Pu, The Journal of Chemical Physics 132 (15) (2010) 154104.

[51] S. Mukherjee, L. Kavalsky, C. V. Singh, Ultrahigh storage and fast diffusion of Na and K in blue phosphorene anodes, ACS Applied Materials & Interfaces 10 (10) (2018) 8630–8639.

[52] A. G. El Hachimi, A. Guillén-López, O. A. Jaramillo-Quintero, M. E. Rincón, P. Y. Sevilla-Camacho, J. Muñiz, Exploring the enhanced performance of Sb_2S_3-doped carbon composites as potential anode materials for sodium-ion batteries: A density functional theory approach, International Journal of Quantum Chemistry 121 (21) (2021) e26779.

[53] S. Mukherjee, A. Banwait, S. Grixti, N. Koratkar, C. V. Singh, Adsorption and diffusion of lithium and sodium on defective rhenium disulfide: A first principles study, ACS Applied Materials & Interfaces 10 (6) (2018) 5373–5384.

[54] Q. Peng, Z. Wang, B. Sa, B. Wu, Z. Sun, Blue Phosphorene/MS_2 (M = Nb, Ta) Heterostructures As Promising Flexible Anodes for Lithium-Ion Batteries, ACS Applied Materials & Interfaces 8 (21) (2016) 13449–13457.

[55] A. Samad, Y.-H. Shin, MoS_2@VS_2 Nanocomposite as a Superior Hybrid Anode Material, ACS Applied Materials & Interfaces 9 (35) (2017) 29942–29949.

[56] D. Er, J. Li, M. Naguib, Y. Gogotsi, V. B. Shenoy, Ti_3C_2 MXene as a High Capacity Electrode Material for Metal (Li, Na, K, Ca) Ion Batteries, ACS Applied Materials & Interfaces 6 (14) (2014) 11173–11179.

[57] G. Henkelman, B. P. Uberuaga, H. Jónsson, A climbing image nudged elastic band method for finding saddle points and minimum energy paths, The Journal of Chemical Physics 113 (22) (2000) 9901–9904.

[58] H. Jónsson, G. Mills, K. W. Jacobsen, Classical and Quantum Dynamics in Con-

densed Phase Simulations, Nudged elastic band method for finding minimum energy paths of transitions, World Scientific, Singapore 3 (1998) 2.

[59] Dudarev, S. L. and Botton, G. A. and Savrasov, S. Y. and Humphreys, C. J. and Sutton, A. P., Electron-energy-loss spectra and the structural stability of nickel oxide: An LSDA+U study, Phys. Rev. B 57 (1998) 1505–1509.

[60] E. German, R. Faccio, A. W. Mombrú, Comparison of standard DFT and Hubbard-DFT methods in structural and electronic properties of TiO_2 polymorphs and H-titanate ultrathin sheets for DSSC application, Applied Surface Science 428 (2018) 118–123.

[61] A. Arnaldsson, W-J. Tang, S. Chill, W-R. Chai and G. Henkelman, "Code Bader Charge Analysis", University of Texas Austin 2020. `http://theory.cm.utexas.edu/henkelman/code/bader/` (2020).

[62] TURBOMOLE V6.6 2014, a development of University of Karlsruhe and Forschungszentrum Karlsruhe GmbH, 1989-2007, TURBOMOLE GmbH, since 2007; available from
`http://www.turbomole.com` (2014).

[63] G. Kresse, J. Hafner, Ab initio molecular dynamics for liquid metals, Phys. Rev. B 47 (1993) 558–561.

[64] G. Kresse, J. Furthmüller, Efficiency of ab-initio total energy calculations for metals and semiconductors using a plane-wave basis set, Computational Materials Science 6 (1) (1996) 15–50.

[65] G. Kresse, D. Joubert, From ultrasoft pseudopotentials to the projector augmented-wave method, Phys. Rev. B 59 (1999) 1758–1775.

[66] H.A. Borbón-Nuñez and J. Muñiz and A.G. El Hachimi and D. Frausto-Silva and J.L. Gutiérrez-Díaz and D. Domínguez and H. Tiznado and A.K. Cuentas-Gallegos, Effect of oxygen based functional groups on the nucleation of TiO_2 by atomic layer deposition: A theoretical and experimental study, Materials Chemistry and Physics 267 (2021) 124588.

[67] W. Yao, J. Zhang, Y. Wang, F. Ren, Hybrid density functional study on the mechanism for the enhanced photocatalytic properties of the ultrathin hybrid layered nanocomposite g-C_3N_4/BiOCl, Applied Surface Science 435 (2018) 1351–1360.

[68] J. Liu, Origin of High Photocatalytic Efficiency in Monolayer g-C_3N_4/CdS Heterostructure: A Hybrid DFT Study, The Journal of Physical Chemistry C 119 (51) (2015) 28417–28423.

[69] C. Delesma, C. Amador-Bedolla, M. Robles, and J. Muñiz, Photoisomerization and its effect in the opto-electronic properties of organic photovoltaic materials: A quantum chemistry study, Journal of Photochemistry and Photobiology A: Chemistry 409 (2021) 113155.

[70] A. S. Nazarloo, M. T. Ahmadian, K. Firoozbakhsh, On the mechanical characteristics of graphene nanosheets: a fully nonlinear modified Morse model, Nanotechnology 31 (11) (2019) 115708.

[71] D. Galhofo, N. Silvestre, B. Faria, C. Guarda, Monotonic and hysteretic in-plane behaviour of graphene through an atomistic FE model, Composites Part B: Engineering 156 (2019) 310–318.

[72] K. Prasert, T. Sutthibutpong, Unveiling the Fundamental Mechanisms of Graphene Oxide Selectivity on the Ascorbic Acid, Dopamine, and Uric Acid by Density Functional Theory Calculations and Charge Population Analysis, Sensors 21 (8) (2021).

[73] D. A. Silva-Alves, M. V. S. Camara, A. M. J. Chaves-Neto, R. Gester, T. Andrade-Filho, Theoretical study of the adsorption of diphenylalanine on pristine graphene, Theoretical Chemistry Accounts 139 (83) (2020) 1–5.

[74] A. Y. Galashev, K. P. Katin, M. M. Maslov, Morse parameters for the interaction of metals with graphene and silicene, Physics Letters A 383 (2) (2019) 252–258.

[75] X.-F. Fan, W. T. Zheng, J.-L. Kuo, D. J. Singh, Adsorption of single Li and the formation of small Li clusters on graphene for the anode of lithium-ion batteries, ACS Applied Materials & Interfaces 5 (16) (2013) 7793–7797.

[76] G.-C. Guo, D. Wang, X.-L. Wei, Q. Zhang, H. Liu, W.-M. Lau, L.-M. Liu, First-principles study of phosphorene and graphene heterostructure as anode materials for rechargeable Li batteries, The Journal of Physical Chemistry Letters 6 (24) (2015) 5002–5008.

[77] X.-X. Wang, C.-M. Tang, X.-F. Zhou, W.-H. Zhu, C. Cheng, Theoretical investigating of graphene/antimonene heterostructure as a promising high cycle

capability anodes for fast-charging lithium ion batteries, Applied Surface Science 491 (2019) 451–459.

[78] F. Tielens, M. Calatayud, A. Beltrán, C. Minot, J. Andrés, Lithium insertion and mobility in the TiO_2-anatase/titanate structure: A periodic DFT study, Journal of Electroanalytical Chemistry 581 (2) (2005) 216–223.

[79] M.L. Ould Ne, A.G. El Hachimi, M. Boujnah, A. Benyoussef and A. El Kenz, Comparative study of electronic and optical properties of graphene and germanene: DFT study, Optik - International Journal for Light and Electron Optics 158 (2018) 693–698.

[80] T. G. Díaz-Rodríguez, M. Pacio, R. Agustín-Serrano, H. Juárez-Santiesteban, J. Muñiz, Understanding structure of small TiO_2 nanoparticles and adsorption mechanisms of PbS quantum dots for solid-state applications: a combined theoretical and experimental study, Theoretical Chemistry Accounts 138 (7) (2019) 92.

[81] M. Ould Ne, A. Abbassi, A. Benyoussef, H. Ez-Zahraouy, A. El Kenz, et al., Electronic optical, properties and widening band gap of graphene with Ge doping, Optical and Quantum Electronics 49 (6) (2017) 1–13.

[82] S. Ding, J. S. Chen, D. Luan, F. Y. C. Boey, S. Madhavi, X. W. D. Lou, Graphene-supported anatase TiO_2 nanosheets for fast lithium storage, Chem. Commun. 47 (2011) 5780–5782.

[83] X.-H. Li, H.-T. Gao, G.-J. Liu, A LDA+U study of the hybrid graphene/anatase

TiO_2 nanocomposites: Interfacial properties and visible light response, Computational and Theoretical Chemistry 1025 (2013) 30–34.

[84] A. El Hachimi, O. Oubram, M. Sadoqi, First-principles study of electronic magnetic and optical properties of black phosphorene adsorbed with Ti and S, Superlattices and Microstructures 146 (2020) 106673.

[85] Q.-F. Li, J.-C. Yang, L. Zhang, Theoretical prediction of blue phosphorene/borophene heterostructure as a promising anode material for lithium-ion batteries, The Journal of Physical Chemistry C 122 (32) (2018) 18294–18303.

[86] X. Zhao, Y. Tian, Z. Lun, Z. Cai, T. Chen, B. Ouyang, G. Ceder, Design principles for zero-strain li-ion cathodes, Joule 6 (7) (2022) 1654–1671.

[87] H. R. Jiang, W. Shyy, M. Liu, L. Wei, M. C. Wu, T. S. Zhao, Boron phosphide monolayer as a potential anode material for alkali metal-based batteries, J. Mater. Chem. A 5 (2017) 672–679.

[88] G. A. Tritsaris, E. Kaxiras, S. Meng, E. Wang, Adsorption and diffusion of lithium on layered silicon for li-ion storage, Nano Letters 13 (5) (2013) 2258–2263.

[89] W.-J. Zhang, A review of the electrochemical performance of alloy anodes for lithium-ion batteries, Journal of Power Sources 196 (1) (2011) 13–24.

[90] J-B. Hou, M. Yang, D-Y. Wang, and J-L. Zhang, Fundamentals and challenges of lithium ion batteries at temperatures between −40 and 60 °C, Advanced Energy Materials 10 (18) (2020) 1904152.

[91] D.-H. Wu, Recent progress of computational investigation on anode materials in Li ion batteries, Frontiers of Physics 6 (2) (2011) 197–203.

[92] C. Spreafico, J. Vande Vondele, Excess Electrons and Interstitial Li Atoms in TiO_2 Anatase: Properties of the (101) Interface, Journal of Physical Chemistry C 119 (27) (2015) 15009–15018.

[93] H. Yildirim, J. Greeley, S. K. Sankaranarayanan, Effect of concentration on the energetics and dynamics of Li ion transport in anatase and amorphous TiO_2, Journal of Physical Chemistry C 115 (31) (2011) 15661–15673.

[94] X. Zhang, Z. Yu, S.-S. Wang, S. Guan, H. Y. Yang, Y. Yao, S. A. Yang, Theoretical prediction of MoN_2 monolayer as a high capacity electrode material for metal ion batteries, J. Mater. Chem. A 4 (2016) 15224–15231.

[95] J. Zhu, U. Schwingenschlögl, P and Si functionalized MXenes for metal-ion battery applications, 2D Materials 4 (2) (2017) 025073.